Proceedings of the 21st ICSMGE, Vienna, Austria, 14 – 19 June 2026. Pistrol, Adam & Schweiger (eds.)
Published by: ÖGG, Austrian Society for Geomechanics, Salzburg, Austria, ISBN 978-3-9503898-4-5
https://doi.org/10.53243/ICSMGE2026-854

Coupled biological-chemical-hydraulic-mechanical model to predict microbially induced calcite precipitation in mine tailing

Alireza Azizi, Kamelia Atefi-Monfared
Department of Civil Engineering, Lassonde School of Engineering, York University, Canada, arazizi@yorku.ca

Paul H. Simms
Civil and Environmental Engineering Department, Carleton University, Canada

ABSTRACT: Tailings, the residual byproducts of mining operations, are typically stored behind manmade containment dams designed to prevent their release to the environment. However, dam failures pose significant risks, unleashing catastrophic volumes of fast-moving slurry that can devastate the ecosystems, infrastructure, and communities. In 2015, failure of Fundao dam in Brazil resulted in 32 m^3 release of waste material to a town, destroyed 158 homes, killed at least 17 people, with the damage of 6.7 billion USD. Microbially Induced Calcite Precipitation (MICP) is an environmentally friendly stabilization technique that utilizes natural microorganisms to produce calcium carbonate, known as bio-cement, which acts as a binding agent. MICP can offer a promising eco-friendly approach for stabilizing mine tailings. However, despite significant advancements in MICP in different applications, its use in mine tailings remains largely unexplored. This is due to two key challenges: the dependency of MICP on multiple factors, including environmental and in-situ conditions, often harsh in mine tailings, and the lack of predictive models to estimate the percentage and extent of cementation and the resulting improvements in the properties of the treated material. The MICP process and the resulting bio-cement production are governed by complex coupled biological-chemical-hydraulic-mechanical (BCHM) processes. A comprehensive analysis is conducted to understand the efficiency of MICP in various in-situ conditions typical in mine tailing repositories. The results indicate that the presence of contaminants reduces the amount of precipitated calcium carbonate, urea concentration, and the extent of biochemical reactions, owing to the inhibitory effects of the contaminants. The outcomes of this study provide insight into the effectiveness of MICP for enhancing the properties of mine tailings and establish a basis for optimizing bio-treatment strategies in contaminated environments, thereby contributing to sustainable mine waste management practices.

KEYWORDS: Microbially Induced Calcite Precipitation (MICP), Coupled Bio-Chemo-Hydro-Mechanical (BCHM) Process.

1 INTRODUCTION

With effective governance, mineral resources hold significant potential to contribute to sustainable development, including the achievement of the Sustainable Development Goals (SDGs) (Pedro et al., 2017). Nonetheless, many resource-rich countries face challenges in converting mineral wealth into long-term, inclusive growth (Carvalho, 2017). Mineral processing generates large volumes of tailings, fine-grained waste materials containing processing water, which are typically stored in surface tailings storage facilities (TSFs) (Kossoff et al., 2014). These TSFs often contain toxic and heavy metal contaminants, presenting substantial environmental risks such as dam failures and groundwater contamination (Wang et al., 2014). The increasing public emphasis on safety and sustainability has driven interest in environmentally friendly alternatives for tailings management (Ait-Khouia et al., 2021).

Recent research has focused on biological methods, particularly Microbially Induced Calcite Precipitation (MICP), as a sustainable ground improvement technique (Aznar-Sánchez et al., 2018). MICP harnesses microbial processes to induce the precipitation of calcium carbonate, enhancing physical properties (DeJong et al., 2006, Mitchell and Santamarina, 2005). Compared to conventional soil stabilization methods, MICP is more sustainable and generates fewer carbon emissions. The urea hydrolysis pathway, which requires urease-producing bacteria, urea, and calcium ions, is recognized as the most efficient route for bio-cementation.

The effectiveness of MICP is influenced by spatial distribution of the precipitated calcite, governed by bacterial and chemical transport processes, which in turn affect pore structure and mechanical properties (Gomez et al., 2018). While several models exist (e.g., (Barkouki et al., 2011, Fauriel and Laloui, 2012, Minto et al., 2019)), many assume simplified or partially coupled systems that do not account for dynamic changes or the impact of contaminants on MICP performance.

In this paper, the MICP process on nature-contaminated tailings has been proposed for the first time by a fully coupled bio-chemo-hydro-mechanical (BCHM) model (Mehrabi and Atefi-Monfared, 2022) to optimize the efficiency in MICP. First, the fully coupled MICP process is modeled and verified, followed by the incorporation of contaminant effects into the respective governing equations for each process. The contaminant transport component has been verified against literature. This work forms part of an ongoing research, with further developments to be reported in an extended study.

2 MATHEMATICAL FRAMEWORK

The governing equations of the model is presented after the assumptions being applied and the final form of the equations are provided due to the page limitations. It is assumed the contaminants are miscible, present in both solid and fluid phases, reactive with a certain decay rate. The fluid phase contaminants are assumed as having been degraded with time, however, in the solid phase it is considered that irreversible biodegradation/ transformation of organic contaminants into products are neglected so the decay rate only appears in the fluid phase balance. It should be noted here that the suggested equations also take an assumption that one severe dominant contaminant exists, which was obtained based on the test outcome of the analysis conducted over the samples.

2.1 *Constitutive equations: Stress-Strain*

Poroelastic theory is adopted for the analysis of the stress-strain behavior of the enhanced sample. The poroelastic model, in the form of the relationships between total induced stress, strain, pore pressure, and precipitated cement volume, is shown in Eq. (1).

$$\sigma_{ij} = 2G\varepsilon_{ij} + \left(K - \frac{2G}{3}\right)\varepsilon_v\delta_{ij} - \alpha p\delta_{ij} - 3K\alpha_c m_c C_c \delta_{ij} \quad (1)$$

σ_{ij} denotes the total induced elastic stress tensor; G and K are the shear and bulk moduli; ε_{ij}, the elastic strain tensor; ε_v, the volumetric strain; δ_{ij}, the Kronecker delta; α, Biot's coefficient; p, induced pore pressure; α_c, volumetric expansion constant for calcium carbonate crystal growth; m_c, molar mass; and C_c, concentration of calcium carbonate. Thus, $\alpha_c m_c C_c$ (m^3/m^3) represents the volumetric precipitated calcium carbonate per unit volume of solid. Although α_c can theoretically be approximated as the inverse of calcium carbonate density, only a fraction contributes to expansion due to significant pore filling.

2.2 *Constitutive equations: Darcy's Law*

To explain the relationship between the fluid flow and pore pressure, Darcy's law was used, as shown in Eq. (2).

$$q = nv_f = -\frac{k}{\mu}(\nabla p + \rho_f g) + nv_s \tag{2}$$

q is Darcy's velocity; v_f and v_s are velocities of fluid and solid phases, respectively; k is intrinsic permeability; μ is dynamic viscosity; g is gravity.

2.3 *Momentum Balance*

Assuming isothermal conditions, and miscible contaminants, the force balance equation is shown in Eqs. (3) to (5).

$$\nabla\sigma + \rho F = 0 \tag{3}$$

$$\rho = (1-n)\rho_s + (n)\rho_f \tag{4}$$

$$\rho_s = (1-S_c)\rho_g + S_c\rho_c \tag{5}$$

σ is the total stress; F is the total body forces; ρ is the total density of the porous media; ρ_s is the density of the solid phase; ρ_g and ρ_c are the densities of grains and calcium carbonate, respectively; S_c is the volume fraction of calcium carbonate.

2.4 *Phase Balance*

The mass balance for component i is demonstrated in Eq. (6).

$$\frac{\partial(nm_i c_i)}{\partial t} + \nabla(nm_i c_i v_i) - \nabla(nD\nabla m_i c_i) + S_i = 0 \tag{6}$$

n is volume fraction of fluid phase, while $(1-n)$ corresponds to solid phase. m_i represents molar mass of chemical components; v_i is velocity vector; D is dispersion-diffusion tensor; and S_i denotes source or sink term.

2.4.1 *Fluid phase balance*

Corresponding transport equations for dissolved urea (same for calcium ions), ammonium, suspended contaminants and bacteria are hence obtained as Eqs. (7)-(10), respectively.

$$\frac{\partial\left(n(m_u C_u)\right)}{\partial t} = -\nabla\left(n(m_u C_u)v_f\right) + \nabla\left(nD\nabla(m_u C_u)\right) - nm_u R_{react} \tag{7}$$

$$\frac{\partial\left(n\left(m_{NH_4^+} C_{NH_4^+}\right)\right)}{\partial t} = -\nabla\left(n\left(m_{NH_4^+} C_{NH_4^+}\right)v_f\right) + \nabla\left(nD\nabla\left(m_{NH_4^+} C_{NH_4^+}\right)\right) + 2nm_{NH_4^+} R_{react} \tag{8}$$

$$\frac{\partial\left(nB_f\right)}{\partial t} = -\nabla\left(nB_f v_f\right) + \nabla\left(nD\nabla B_f\right) - nB_f R_{attach} - nB_f R_{decay} \tag{9}$$

$$\frac{\partial(n(C_{con}))}{\partial t} = -\nabla\left(nv_f C_{con}\right) + \nabla(nD\nabla C_{con}) - \lambda_{con} n C_{con} \tag{10}$$

B_f is the concentration of suspended bacteria; m_u, $m_{Ca^{+2}}$, and $m_{NH_4^+}$ are the molar masses of dissolved urea, calcium, and ammonium ions, respectively. λ_{con} denotes the contaminant decay rate, reflecting the irreversible biodegradation or transformation of organic contaminants. R_{react} (Eq. (11)) is the rate of chemical species consumption or production per pore volume due to biochemical reactions. Contaminants can suppress urease activity, following enzyme kinetics (Cook and Cleland, 2007). R_{attach} is the rate at which bacteria attach to solid grains, and R_{decay} is the bacterial decay rate.

$$R_{react} = R_{max}\frac{C_u}{K_m\left(1+\frac{C_{con}}{K_{i,con}}\right)+C_u}\exp\left(-\frac{t}{t_{max}}\right) \tag{11}$$

R_{max} is maximum reaction rate; K_m is half-saturation constant for urea, $K_{i,con}$ is contaminants inhibition constant, t is treatment duration and t_{max} is maximum active time of bacteria.

2.4.2 *Solid phase balance*

Assuming the volume fraction of the solid phase as $(1-n)$, the mass balances for grains, calcium carbonate, attached bacteria, and contaminants can be expressed as Eqs. (12) to (15).

$$\frac{\partial\left((1-n)(1-S_c)\rho_g\right)}{\partial t} = -\nabla\left((1-n)(1-S_c)\rho_g v_s\right) \tag{12}$$

$$\frac{\partial\left((1-n)(S_c)\rho_c\right)}{\partial t} = -\nabla\left((1-n)(S_c)\rho_c v_s\right) + nm_c R_{react} \tag{13}$$

$$\frac{\partial\left((1-n)B_s\right)}{\partial t} = -\nabla\left((1-n)B_s v_s\right) + nR_{attach}B_f - (1-n)R_{decay}B_s \tag{14}$$

$$\frac{\partial\left((1-n)(\rho_{con}C_{con})\right)}{\partial t} = -\nabla((1-n)v_s\rho_{con}C_{con}) + nm_{con}R_{react,\,con} \tag{15}$$

2.5 *Bio-cement induced hydro-mechanical changes*

2.5.1 *Stiffness*

Stiffness changes as a result of bio-cementation can be predicted using an empirical correlation suggested by Van Paassen et al., (van Paassen et al., 2010). Shear and bulk moduli can be estimated as functions of cementation, as represented in Eqs. (16). MICP enhances the stiffness of the porous medium (Gomez et al., 2018), and this effect is incorporated into the governing equations by defining the shear and bulk moduli as functions of the precipitated calcium carbonate content.

$$G = G_0\left(1+\frac{9.7}{152}m_c C_c\right)^2;\; K = K_0\left(1+\frac{9.7}{152}m_c C_c\right)^2 \tag{16}$$

G_0 and K_0 are initial shear and bulk moduli, G and K are the shear and bulk moduli of the cemented sample, respectively; C_c is cement content.

2.5.2 *Porosity*

Precipitation of calcium carbonate cause porosity changes, as Eq. (17). The first term accounts for porosity changes through hydro-mechanical deformation, whereas the second term is for pore filling via calcium carbonate precipitation.

$$\frac{\partial n}{\partial t} = (1-n)\frac{\partial}{\partial t}(\nabla u) - \frac{(1-n)}{1-S_c}\frac{\partial S_c}{\partial t} \tag{17}$$

2.5.3 *Permeability*

To relate porosity and intrinsic permeability, Kozeny-Carman relationship is used as shown in Eq. (18).

$$k = \left(\frac{(d_{50})^2}{180}\right) \times \left(\frac{n^3}{(1-n)^2}\right) \tag{18}$$

Where d_{50} is the mean particle size of the sample.

2.6 *Field equations*

2.6.1 *Chemo-hydro-mechanical equilibrium*

Elastic horizontal deformation at a point in time and space can be shown in terms of radial displacement within an elastic media. Substituting Eq. (1) into the balance equations of forces (3) and (4), and re-expressing the components of strain in terms of displacement, Eqs. (19) and (20) are obtained.

$$\frac{\partial}{\partial r}\left[\left(K+\frac{4G}{3}\right)\left(\frac{\partial u_r}{\partial r}\right)+\left(K-\frac{2G}{3}\right)\left(\frac{u_r}{r}+\frac{\partial u_z}{\partial z}\right)\right] + \frac{1}{r}\left[2G\left(\frac{\partial u_r}{\partial r}-\frac{u_r}{r}\right)\right] = \frac{\partial}{\partial r}[\alpha p + 3K\alpha_c m_c C_c] \tag{19}$$

$$\frac{\partial}{\partial z}\left[\left(K+\frac{4G}{3}\right)\left(\frac{\partial u_z}{\partial z}\right)+\left(K-\frac{2G}{3}\right)\left(\frac{u_r}{r}+\frac{\partial u_r}{\partial r}\right)\right] = \frac{\partial}{\partial z}[\alpha p + 3K\alpha_c m_c C_c] - \rho g \tag{20}$$

2.7 *Transport equation*

2.7.1 *Chemical species*

Given the dependence of the reaction rate on urea concentration, it is necessary to solve the corresponding differential equation. The porosity variation term in Eq. (7) is replaced with the expression derived from the fluid continuity equation. The density-driven flow term is omitted due to its negligible contribution compared to advection and dispersion. This formulation yields the governing equations for urea (same as dissolved calcium), dissolved calcium, and ammonium concentrations.

$$\frac{\partial C_u}{\partial t} = -\left(\frac{q}{n}\right)\nabla C_u + \nabla.(D.\nabla C_u) - R_{react} \tag{21}$$

$$\frac{\partial C_{NH_4^+}}{\partial t} = -\left(\frac{q}{n}\right)\nabla C_{NH_4^+} + \nabla.\left(D.\nabla C_{NH_4^+}\right) + 2R_{react} \tag{22}$$

By replacing porosity changes according to Eq. (13) with those from Eq. (17), and disregarding density-driven flow, an expression for calcium carbonate concentration is obtained as Eq. (23). In this equation, the first term within the right-hand side is the precipitation of calcium carbonate due to urea hydrolysis. The second term is the impact of porosity changes on calcium carbonate concentration.

$$\frac{\partial C_c}{\partial t} = \left(\frac{n}{1-n}\right)R_{react} - \left(\frac{m_c}{\rho_c}\right)\left(\frac{n}{1-n}\right)R_{react}C_c \tag{23}$$

Porosity variations, defined by the fluid volume fraction (n), inherently affect the solid phase $(1-n)$ and thus influence the concentration of precipitated calcium carbonate relative to the solid volume.

2.7.2 *Bacteria*

Ignoring the density-driven flow, the concentration of suspended bacteria can be determined as shown in Eq. (24).

$$\frac{\partial B_f}{\partial t} = -\left(\frac{q}{n}\right)\nabla B_f + \nabla.\left(D.B_f\right) - R_{attach}B_f - R_{decay}B_f \tag{24}$$

The concentration of attached bacteria is obtained by rearranging Eq. (14). In Eq. (25) the first term on the right-hand side represents the rate of bacterial attachment to the solid phase, whereas the second term accounts for the influence of porosity variation (n) on the concentration of adsorbed bacteria.

$$\frac{\partial B_s}{\partial t} = \left(\frac{n}{1-n}\right)R_{attach}B_f - \left(\frac{m_c}{\rho_c}\right)\left(\frac{n}{1-n}\right)R_{react}B_s - R_{decay}B_s \tag{25}$$

2.7.3 *Contaminants*

Co-precipitation of MCO_3 in the solid phase resulting from the reaction between dissolved metal and carbonate ions is demonstrated in Eq. (26). The pre-factor $\frac{n}{1-n}$ in the first term in the right hand-side transforms a pore volume-based rate to a solid volume-based concentration. Second term accounts for porosity changes (pore filling) that rescale the reference volume of the solid phase. Here m_{con} and ρ_{con} are the molar mass and density of the contaminant.

$$\frac{\partial C_{con}}{\partial t} = \left(\frac{n}{1-n}\right)R_{react,con} - \left(\frac{m_{con}}{\rho_{ccon}}\right)\left(\frac{n}{1-n}\right)R_{react,con}C_{con} \tag{26}$$

2.7.4 *Flow equations*

Incorporating the pressure-dependent variation of fluid density via the definition of a compressibility coefficient allows the mass balance equation for pore water to be simplified, resulting in Eq. (27), which expresses the general form of the flow equation.

$$\frac{\partial n}{\partial t} = -\frac{n}{K_f}\frac{\partial \rho_f}{\partial t} - \nabla.\left(n v_f\right) \tag{27}$$

Formulating the grain mass balance with grain compressibility defines the model's hydro-mechanical component. Grain density variations, dependent on stress and pore pressure, are integrated with Darcy's law, calcium carbonate changes, and the time-dependent σ expression to derive the general fluid flow equation (Eq. (28)).

$$\frac{k}{\mu}\nabla.\left(\nabla p + \rho_f g\right) - \left(\frac{n}{K_f}+\frac{\alpha-n}{K_g}\right)\frac{\partial p}{\partial t} = \alpha\frac{\partial}{\partial t}(\nabla.u) - n\frac{m_c}{\rho_c}R_{react} \tag{28}$$

3 METHODOLOGY

Calcium carbonate $CaCO_3$ and/or metal carbonate (MCO_3) precipitation forms a biocement matrix by linking $CaCO_3$ precipitates (Wilcox et al., 2024). At the microscale, precipitates uniformly form around soil particles or at contacts, filling pores or creating interparticle bridges through capillary forces (Mehrabi and Atefi-Monfared, 2025). Both mechanisms reduce pore space, lowering hydraulic conductivity (Mujah et al., 2017). Accumulated precipitates also reduce void space and enhance interparticle cohesion, decreasing permeability and inducing a plugging effect (Zúñiga-Barra et al., 2022). These interparticle bridges are further believed to improve mechanical performance, notably by increasing shear strength (Mujah et al., 2017).

MICP contributes to the remediation of metal(loid) contamination through several mechanisms, including contaminant removal, immobilization, the creation of impermeable barriers, and reduction of soil liquefaction potential. Removal occurs via the direct precipitation of $CaCO_3$ and MCO_3 minerals, whereas immobilization is associated with the reduction of leachate as a result of MICP activity (Zúñiga-

Barra et al., 2022). Leachate reduction is typically indicated by a decrease in the soluble-exchangeable fraction, which reflects contaminant bioavailability and mobility (Achal et al., 2012). Additional reduction in leachate occurs through the deposition and clogging of pore spaces by $CaCO_3$ crystals (Proudfoot et al., 2022). The development of the biocement matrix also facilitates the formation of an impermeable barrier, effectively producing a plugging effect (Kang et al., 2014).

More specifically, MICP-based remediation can proceed via direct mechanisms, such as the fixation of contaminants within $CaCO_3$ or MCO_3 precipitates (Achal et al., 2013), or indirect mechanisms, including the formation of metal(loid)-$CaCO_3$ complexes (Wilcox et al., 2024), incorporation of contaminants into the crystal lattice (Govarthanan et al., 2013), and sorption processes (Kang et al., 2014). Incorporation into the crystal structure occurs when divalent cations, possessing similar ionic radii and charges to Ca^{2+}, are substituted into the lattice via ion exchange or are entrapped within fissures and interstices (Achal et al., 2011). In addition, sorption refers to the adsorptive capacity of $CaCO_3$, which has been extensively utilized for the removal of metal(loid)s from aqueous systems. The primary mechanisms by which contaminants influence the MICP process are summarized in Table 1, however, in this study only the inhibition of bacterial activity and the transport of contaminants are implemented.

Table 1. Mapping contaminants effects.

Effects	Mechanistic model	Impacts on MICP
Reaction of contaminants with carbonate ions	*Chemical precipitation kinetics*	Reduces carbonate availability, lowers $CaCO_3$ precipitation
Inhibition of bacterial activity	*Enzyme inhibition model*	Lowers urea hydrolysis rate, reducing carbonate production
Degradation of contaminants by microbial enzymes	*Michaelis-Menten model*	Reduces contaminants concentration, lowering inhibition effects over time
Contaminants transported out of the matrix	*Transport equations*	Concentration is reduced

A finite element (FE) model was developed to simulate the coupled BCHM processes controlling MICP in a soil column, based on the framework and assumptions by Mehrabi and Atefi-Monfared (Mehrabi and Atefi-Monfared, 2022). The model represents a 1D column, 16 cm height and 6.6 cm in diameter, representing lab-scale bio-cementation. The porous medium is considered isothermal, elastic, homogeneous, and fully saturated, comprising a solid phase (soil particles, attached bacteria, and $CaCO_3$) and a fluid phase (pore water, suspended bacteria, and dissolved urea, calcium, and ammonium). Subscripts "s" and "f" refer to solid and fluid phases, respectively.

The fluid phase is considered compressible, with no internal generation of pore water. Advective transport is modeled using Darcy's law, while non-advective transport is described by Fick's law. Adsorption of dissolved species onto solid surfaces and density-driven flow arising from fluid density variations are neglected due to their negligible impact (Van Wijngaarden et al., 2011, Van Wijngaarden et al., 2013). For the solid phase, dispersion–diffusion is disregarded in comparison to advection. The influence of surface-bound bacteria on porosity is assumed negligible, supported by experimental evidence indicating that biofilm growth is unlikely within the short timeframes considered (Wang and Nackenhorst, 2020).

Biochemical interactions are modeled as irreversible, first-order reactions driven by urease activity from both attached and suspended bacteria, alongside dissolved urea concentration. Secondary effects like pH and temperature are considered negligible compared to bacterial activity and urea availability (Wang and Nackenhorst, 2020). Gravitational effects are included. Bacterial attachment is flow-velocity-dependent, stopping beyond a critical velocity. A positive sign convention is used for compressive stresses, and simulations assume plane strain. Internal/external body forces and inertial effects are excluded, consistent with standard BCHM modeling.

Due to the strong coupling between displacement and pore pressure, the flow and equilibrium equations of the CHM subsystem are solved simultaneously. Bacterial transport equations are then solved, with their outputs feeding into the chemical species transport equations. These results are reintroduced into the CHM model. The updated CHM flow properties serve as input for the next simulation step, allowing iterative evaluation of bacterial and chemical transport.

Constant injection rates and specified initial concentrations of bacteria, urea, and calcium ions are applied at the injection boundary. The lower boundary is mechanically fixed with zero pore pressure to simulate drainage. Initially, the concentrations of all chemical species and bacteria are set to zero; however, contaminants are present within the medium as inherent material properties. Hydrostatic pore pressure is established throughout the column. Characteristic parameters and boundary conditions are adapted from Fauriel and Laloui for the BCHM model (Fauriel and Laloui, 2012) to ensure methodological consistency. The treatment sequence consists of water injection from the top at a constant rate until steady-state flow is reached, a 30-minute bacterial injection phase, a 30-minute closed-system phase to allow bacterial attachment, a five-hour injection of urea/calcium solution, followed by a two-hour closed phase to enable calcium carbonate precipitation. Throughout the entire process, contaminants are present in the medium. The model input parameters are listed in Table 2.

Table 2. Input parameters for the BCHM FE model.

Parameter	Input
$K\ (MPa);\ G\ (MPa);\ K_f\ (GPa);\ K_g\ (GPa)$	100; 75; 2; 80
$\rho_g\ (kg/m^3);\ \rho_w\ (kg/m^3)$	2600; 1000
$\alpha;\ \alpha_c;\ n_0;\ k_0;\ K_m$	1; 0; 0.4; 2×10^{-12}; 0.01
$C_0\ (kmol/m^3);\ q_{inj}^c\ (m/s);\ \mu\ (Pa.s)$	0.5, 1×10^{-5}; 1×10^{-3}
$\rho_c\ (kg/m^3);\ m_c\ (kg/kmol)$	1400; 100.1
$D_{diff}\ (m^2/s);\ \alpha_T\ (m);\ \alpha_L\ (m)$	2×10^{-9}; 2×10^{-3}; 1×10^{-3}
$B_0\ (OD);\ u_b\ (kmol/m^3.sOD)$	3; 2×10^{-5}
$t_{max}\ (s);\ K_{attach}\ (1/s)$	28800; 3×10^{-4}

Input parameters for the coupled contaminant model (BCHM+C) are identical to the BCHM, but the contaminants' characteristics are given based on a lead (Pb) contaminated tailings study (Chen et al., 2022) as presented in Table 3. Pb is one of the most inhibitor chemicals to the urease activity, commonly found in tailings. The inhibition of Pb on urease activity was inputted from (Zaborska et al., 2004).

Table 3. Parameters for the BCHM+C FE model.

Parameter	Input
Concentration of contaminant, $C_{con}\ (mg/L)$	10800
Decay rate, $\lambda\ (1/s)$	0.001
Inhibition constant, $K_i\ (\mu M)$	80

4 RESULTS AND DISCUSSIONS

4.1 *Verification*

4.1.1 *Coupled BCHM model*

Our current BCHM model, has been verified against one of the most sophisticated frameworks in literature by Fauriel and Laloui (Fauriel and Laloui, 2012). The current model, however, involves calcium carbonate precipitation and variation of in-situ stress due to growth of calcium carbonate. The model by Fauriel and Laloui supposes that the attaching rate of bacteria is not dependent upon fluid velocity and is constant, as contrasted with this current model that supposes this attaching rate to be velocity dependent. As shown in Figure 1, Fauriel and Laloui's data are included in the graphs, for verification purposes, as a reference to correlate both models' outcomes.

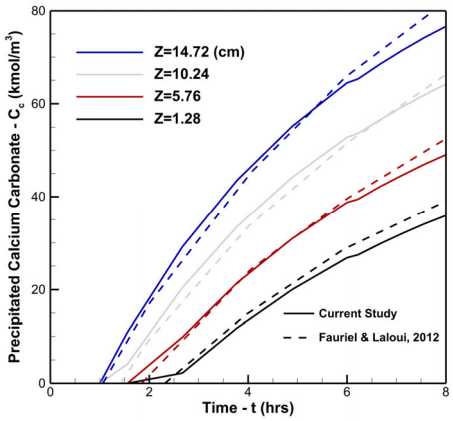

Figure 1. Calcium carbonate changes at various axial distances (Z) from the injection boundary.

4.1.2 *Contaminant transport model*

Transport of contaminants, an aspect of their effects, is verified against Zhao et al. (Zhao et al., 1994) and an analytical solution provided by Van Genuchten et al. (Van Genuchten, 1982). The verification is presented in Figure 2.

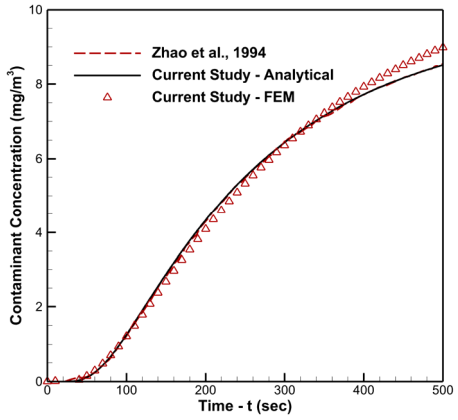

Figure 2. Verification of contaminant transport model.

4.2 *Coupled BCHM model incorporating contaminants*

The coupled BCHM model was extended to incorporate the effects of contaminants, primarily through the inhibition of microbial activity. The presence of contaminants can reduce the quantity of precipitated calcium carbonate by suppressing the biochemical reactions, as illustrated in Figure 3. Contamination lowers both the initial slope and the final value. Figure 4 shows the effective rate is smaller having same biomass, because of increase in inhibition. The contaminant concentration and its associated inhibition constant are the two primary parameters governing the extent to which the contaminant impedes the reactions, and consequently, the precipitation of biocement.

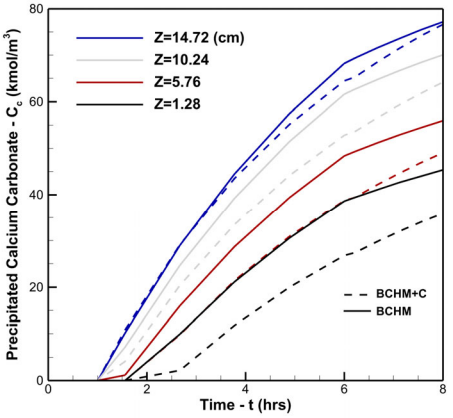

Figure 3. Calcium carbonate changes at various axial distances (Z) from the injection boundary.

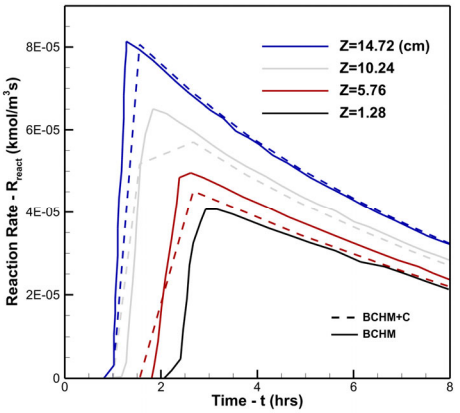

Figure 4. Reaction rate changes with axial distance (Z) from the injection boundary for uncontaminated and contaminated samples.

Figure 5 presents the temporal variation of urea concentration based on the Eq. (7). Urea concentration in pores is affected by advection, diffusion, dispersion, and microbial consumption. Contaminants further reduce urea levels compared to clean sand, limiting microbial activity and potentially reducing the efficiency of the bio-cementation process.

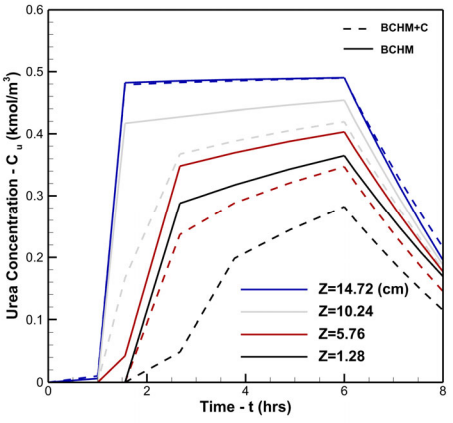

Figure 5. Urea variation with axial distance (Z) from the injection boundary for uncontaminated and contaminated samples.

5 CONCLUSIONS

A coupled biological-chemical-hydraulic-mechanical model was verified to predict biocement distribution and improved properties of MICP-treated samples. The model introduces a

novel feature by incorporating contaminant effects on the MICP process, which can inhibit bacterial activity, clog pores, and degrade. The next step, which is currently ongoing, involves performing experimental investigations to assess the model's predictability.

6 ACKNOWLEDGMENTS

The authors gratefully acknowledge the financial support of this research by Natural Sciences and Engineering Research Council of Canada (NSERC).

7 REFERENCES

ACHAL, V., PAN, X., FU, Q. & ZHANG, D. 2012. Biomineralization based remediation of As (III) contaminated soil by Sporosarcina ginsengisoli. *Journal of hazardous materials,* 201**,** 178-184.

ACHAL, V., PAN, X., LEE, D.-J., KUMARI, D. & ZHANG, D. 2013. Remediation of Cr (VI) from chromium slag by biocementation. *Chemosphere,* 93**,** 1352-1358.

ACHAL, V., PAN, X. & ZHANG, D. 2011. Remediation of copper-contaminated soil by Kocuria flava CR1, based on microbially induced calcite precipitation. *Ecological Engineering,* 37**,** 1601-1605.

AIT-KHOUIA, Y., BENZAAZOUA, M. & DEMERS, I. 2021. Environmental desulfurization of mine wastes using various mineral processing techniques: Recent advances and opportunities. *Minerals Engineering,* 174**,** 107225.

AZNAR-SÁNCHEZ, J. A., GARCÍA-GÓMEZ, J. J., VELASCO-MUÑOZ, J. F. & CARRETERO-GÓMEZ, A. 2018. Mining waste and its sustainable management: advances in worldwide research. *Minerals,* 8**,** 284.

BARKOUKI, T. H., MARTINEZ, B. C., MORTENSEN, B., WEATHERS, T., DE JONG, J., GINN, T., SPYCHER, N., SMITH, R. & FUJITA, Y. 2011. Forward and inverse bio-geochemical modeling of microbially induced calcite precipitation in half-meter column experiments. *Transport in Porous Media,* 90**,** 23-39.

CARVALHO, F. P. 2017. Mining industry and sustainable development: time for change. *Food and Energy security,* 6**,** 61-77.

CHEN, T., WEN, X.-C., ZHANG, L.-J., TU, S.-C., ZHANG, J.-H., SUN, R.-N. & YAN, B. 2022. The geochemical and mineralogical controls on the release characteristics of potentially toxic elements from lead/zinc (Pb/Zn) mine tailings. *Environmental Pollution,* 315**,** 120328.

COOK, P. F. & CLELAND, W. W. 2007. *Enzyme kinetics and mechanism*, Garland Science.

DEJONG, J. T., FRITZGES, M. B. & NÜSSLEIN, K. 2006. Microbially induced cementation to control sand response to undrained shear. *Journal of geotechnical and geoenvironmental engineering,* 132**,** 1381-1392.

FAURIEL, S. & LALOUI, L. 2012. A bio-chemo-hydro-mechanical model for microbially induced calcite precipitation in soils. *Computers and Geotechnics,* 46**,** 104-120.

GOMEZ, M. G., DEJONG, J. T. & ANDERSON, C. M. 2018. Effect of bio-cementation on geophysical and cone penetration measurements in sands. *Canadian Geotechnical Journal,* 55**,** 1632-1646.

GOVARTHANAN, M., LEE, K.-J., CHO, M., KIM, J. S., KAMALA-KANNAN, S. & OH, B.-T. 2013. Significance of autochthonous Bacillus sp. KK1 on biomineralization of lead in mine tailings. *Chemosphere,* 90**,** 2267-2272.

KANG, C.-H., HAN, S.-H., SHIN, Y., OH, S. J. & SO, J.-S. 2014. Bioremediation of Cd by microbially induced calcite precipitation. *Applied biochemistry and biotechnology,* 172**,** 2907-2915.

KOSSOFF, D., DUBBIN, W., ALFREDSSON, M., EDWARDS, S., MACKLIN, M. & HUDSON-EDWARDS, K. A. 2014. Mine tailings dams: Characteristics, failure, environmental impacts, and remediation. *Applied geochemistry,* 51**,** 229-245.

MEHRABI, R. & ATEFI-MONFARED, K. 2022. A coupled bio-chemo-hydro-mechanical model for bio-cementation in porous media. *Canadian Geotechnical Journal,* 59**,** 1266-1280.

MEHRABI, R. & ATEFI-MONFARED, K. 2025. Comparative Analysis of Silt, Kaolinite, and Montmorillonite Particle Effects on Bio-cementation in Sandy Soils. *Canadian Geotechnical Journal*.

MINTO, J. M., LUNN, R. J. & EL MOUNTASSIR, G. 2019. Development of a reactive transport model for field-scale simulation of microbially induced carbonate precipitation. *Water Resources Research,* 55**,** 7229-7245.

MITCHELL, J. K. & SANTAMARINA, J. C. 2005. Biological considerations in geotechnical engineering. *Journal of geotechnical and geoenvironmental engineering,* 131**,** 1222-1233.

MUJAH, D., SHAHIN, M. A. & CHENG, L. 2017. State-of-the-art review of biocementation by microbially induced calcite precipitation (MICP) for soil stabilization. *Geomicrobiology Journal,* 34**,** 524-537.

PEDRO, A., AYUK, E. T., BODOUROGLOU, C., MILLIGAN, B., EKINS, P. & OBERLE, B. 2017. Towards a sustainable development licence to operate for the extractive sector. *Mineral Economics,* 30**,** 153-165.

PROUDFOOT, D., BROOKS, L., GAMMONS, C. H., BARTH, E., BLESS, D., NAGISETTY, R. M. & LAUCHNOR, E. G. 2022. Investigating the potential for microbially induced carbonate precipitation to treat mine waste. *Journal of hazardous materials,* 424**,** 127490.

VAN GENUCHTEN, M. T. 1982. *Analytical solutions of the one-dimensional convective-dispersive solute transport equation*, US Department of Agriculture, Agricultural Research Service.

VAN PAASSEN, L. A., GHOSE, R., VAN DER LINDEN, T. J., VAN DER STAR, W. R. & VAN LOOSDRECHT, M. C. 2010. Quantifying biomediated ground improvement by ureolysis: large-scale biogrout experiment. *Journal of geotechnical and geoenvironmental engineering,* 136**,** 1721-1728.

VAN WIJNGAARDEN, W., VERMOLEN, F., VAN MEURS, G. & VUIK, C. 2011. Modelling biogrout: a new ground improvement method based on microbial-induced carbonate precipitation. *Transport in porous media,* 87**,** 397-420.

VAN WIJNGAARDEN, W., VERMOLEN, F., VAN MEURS, G. & VUIK, C. 2013. A mathematical model for biogrout: bacterial placement and soil reinforcement. *Computational Geosciences,* 17**,** 463-478.

WANG, C., HARBOTTLE, D., LIU, Q. & XU, Z. 2014. Current state of fine mineral tailings treatment: A critical review on theory and practice. *Minerals Engineering,* 58**,** 113-131.

WANG, X. & NACKENHORST, U. 2020. A coupled bio-chemo-hydraulic model to predict porosity and permeability reduction during microbially induced calcite precipitation. *Advances in water resources,* 140**,** 103563.

WILCOX, S. M., MULLIGAN, C. N. & NECULITA, C. M. 2024. Microbially Induced Calcium Carbonate Precipitation as a Bioremediation Technique for Mining Waste. *Toxics,* 12**,** 107.

ZABORSKA, W., KRAJEWSKA, B. & OLECH, Z. 2004. Heavy metal ions inhibition of jack bean urease: potential for rapid contaminant probing. *Journal of Enzyme Inhibition and Medicinal Chemistry,* 19**,** 65-69.

ZHAO, C., XU, T. & VALLIAPPAN, S. 1994. Numerical modelling of mass transport problems in porous media: A review. *Computers & structures,* 53**,** 849-860.

ZÚÑIGA-BARRA, H., TOLEDO-ALARCÓN, J., TORRES-ARAVENA, Á., JORQUERA, L., RIVAS, M., GUTIÉRREZ, L. & JEISON, D. 2022. Improving the sustainable management of mining tailings through microbially induced calcite precipitation: a review. *Minerals Engineering,* 189**,** 107855.